

Exploring \tilde{R}_2 Leptoquarks and Majorana Neutrinos via same-sign dimuons at the HL-LHC.

Subham Saha,^{1,2,*} Arvind Bhaskar,^{1,2,†} and Manimala Mitra^{1,2,‡}

¹*Institute of Physics, Sachivalaya Marg, Bhubaneswar, Odisha 751005, India*

²*Homi Bhabha National Institute, BARC Training School Complex, Anushakti Nagar, Mumbai 400094, India*

We study the phenomenology of scalar leptoquark (sLQ) \tilde{R}_2 coupled to right-handed neutrinos (RHNs) at the High-Luminosity Large Hadron Collider (HL-LHC), focusing on signatures that depart from those targeted by conventional sLQ searches at the LHC. If sLQ is heavier than the RHN, for $\mathcal{O}(1)$ Yukawa, the decay of sLQ to RHN and jet can dominate, leading to distinctive final states that are only weakly constrained by existing analysis. We consider the same sign dimuon and multi-jet signature. This is particularly a unique and clean lepton-number violating signature, benefiting from low Standard Model backgrounds and directly sensitive to the Majorana nature of the RHN. A comprehensive analysis is performed by combining the sLQ pair and single production mechanisms at $\sqrt{s} = 14$ TeV, allowing us to assess the sensitivity reach of HL-LHC over a wide range of sLQ masses and Yukawa couplings. We demonstrate that pair production dominates the sensitivity at the TeV scale, while single production becomes increasingly important for multi-TeV sLQ masses, enabling the HL-LHC to probe regions of parameter space beyond the reach of current direct and indirect constraints. Our results highlight the strong complementarity between production modes and emphasize the unique capability of the HL-LHC to test sLQ scenarios involving RHNs. The framework presented here provides a well-motivated target for future experimental searches and offers a pathway toward simultaneously probing sLQ dynamics and parameter space of a Majorana RHN.

I. INTRODUCTION

Leptoquarks (LQs) constitute a well-motivated class of hypothetical particles that arise in a wide range of theoretical frameworks aiming at a unified description of quarks and leptons [1–4]. As color-triplet bosons carrying both baryon and lepton quantum numbers, they provide a natural link between the two fermionic sectors of the Standard Model (SM) and can offer a possible explanation for its observed generational structure. LQs appear generically in various beyond standard model (BSM) theories such as, Pati-Salam models [5], SU(5) grand unified theories [6], the models with quark lepton compositeness [7], R -parity violating supersymmetric models [8] or coloured Zee-Babu model [9] etc. Beyond their theoretical appeal, LQs have attracted renewed phenomenological interest in recent years due to their potential to address persistent experimental anomalies, notably in semileptonic B -meson decays [10] and in the anomalous magnetic moment of the muon [11].

The Large Hadron Collider (LHC) has played a central role in the experimental search for LQs. The ATLAS and CMS collaborations have placed stringent exclusion limits on their masses, extending up to the TeV scale for a variety of LQ representations. These searches are optimized for final states with high-transverse momentum leptons and jets, corresponding to the conventional LQ decay into a charged lepton and a quark [12]. Indirect constraints on the LQ couplings to SM quarks and leptons are further obtained from high- p_T dilepton and monolepton plus missing transverse momentum searches at colliders [13–19]. Nevertheless, several

theoretically well-motivated decay modes remain only weakly constrained. In particular, scenarios in which LQs couple to right-handed neutrinos (RHNs) are of special interest [20–24]. RHNs are a minimal and well-established extension of the SM that can naturally account for the smallness of observed neutrino masses through the seesaw mechanism [25–29].

If the sLQ is heavier than the associated RHN, the decay of sLQ to RHN and a jet becomes a dominant production mode. This possibility dramatically alters the expected collider signatures, significantly modifying existing bounds derived from conventional LQ searches and opening up a largely unexplored region of parameter space. The subsequent decay of the RHN can lead to distinctive multi-lepton and multi-jet final states with rich phenomenology. Although our earlier work investigated the discovery prospects of sLQs in a future high-energy muon collider [30], the High-Luminosity LHC (HL-LHC) [31] offers an immediate and complementary opportunity to probe such scenarios. The large integrated luminosity anticipated at the HL-LHC enables sensitive searches for rare processes that are otherwise inaccessible at the current LHC.

In this study, we focus on a particularly clean and striking collider signature: the production of sLQs followed by decays into RHN. If the RHN is Majorana in nature, it can induce same-sign dimuon final states accompanied by multiple jets, $\mu^\pm \mu^\pm + \text{jets}$. This final state benefits from exceptionally low SM backgrounds, making it a powerful probe of new physics. The observation of a statistically significant excess of same sign dimuon events would therefore constitute a smoking-gun signature not only for sLQ interactions but also for the Majorana nature of the RHN. In what follows, we present a dedicated HL-LHC study of this channel. We develop an optimized search strategy and assess the discovery potential of HL-LHC in probing TeV-scale sLQ coupling to

* subham.saha@iopb.res.in

† arvind.bhaskar@iopb.res.in

‡ manimala@iopb.res.in

RHNs.

The rest of this paper is organized as follows. In Section II, we introduce the sLQ model under consideration and define the relevant interactions. Section III discusses the possible decay modes of the LQ and RHN. In Section IV, we enumerate the LQ production mechanisms at the HL-LHC that contribute to the same sign dimuon plus multijet final state. The signal definition, relevant SM backgrounds, and the event selection strategy are described in Section V. The statistical framework and analytical expressions used to evaluate signal significance are outlined in Section VI. Our results are presented in Section VII, followed by our conclusions in Section VIII.

II. MODEL

To facilitate our analysis, we extend the SM by introducing two new particles: sLQ doublet, \tilde{R}_2 with quantum numbers $(\mathbf{3}, \mathbf{2}, 1/6)$ and three right-handed neutrinos, N which is a singlet $(\mathbf{1}, \mathbf{1}, 0)$ under the SM. The isospin components of the \tilde{R}_2 doublet can be written as $\tilde{R}_2 = (\tilde{R}_2^{2/3}, \tilde{R}_2^{-1/3})$. The most general, renormalizable Lagrangian describing the interactions of the \tilde{R}_2 LQ with SM fermions and the RHN, following the notation in [1, 4, 21], is given as:

$$\mathcal{L}_{\text{LQ}} = -Y_{ij} \bar{d}_R^i \tilde{R}_2^a \varepsilon^{ab} L_L^{j,b} + Z_{ij} \bar{Q}_L^{i,a} \tilde{R}_2^a N_R^j + \text{H.c.}, \quad (1)$$

Here $i, j = 1, 2, 3$ are the generation indices, $a, b = 1, 2$ are $SU(2)_L$ indices and ε^{ab} is the $SU(2)$ antisymmetric tensor. The matrices Y_{ij} and Z_{ij} contain the Yukawa couplings. When expanded, this Lagrangian yields the interaction terms for the component fields:

$$\begin{aligned} \mathcal{L}_{\text{LQ}} = & -Y_{ij} \bar{d}_R^i e_L^j \tilde{R}_2^{2/3} + (Y U_{\text{PMNS}})_{ij} \bar{d}_R^i \nu_L^j \tilde{R}_2^{-1/3} \\ & + (V_{\text{CKM}} Z)_{ij} \bar{u}_L^i N_R^j \tilde{R}_2^{2/3} + Z_{ij} \bar{d}_L^i N_R^j \tilde{R}_2^{-1/3} + \text{H.c.} \end{aligned} \quad (2)$$

In the above equation, U_{PMNS} and V_{CKM} are the Pontecorvo-Maki-Nakagawa-Sakata (PMNS) and Cabibbo-Kobayashi-Maskawa (CKM) mixing matrices, respectively. For simplicity and to focus on the novel signature involving RHNs, we will consider a scenario with minimal flavor assumptions. We consider Yukawa couplings Y_{12} that quantifies the coupling strength of a sLQ, first generation quark and a second generation lepton and Z_{11} that quantifies the coupling strength of a sLQ, first generation quark and a first generation RHN. The first generation RHN, assumed to be a Majorana fermion is denoted as N . In addition to its Yukawa interaction with the sLQ, we consider that N mixes with the SM muon neutrino ν_μ , through an active-sterile mixing angle, $V_{\mu N}$. This mixing induces interactions between the RHN and the SM electroweak bosons (W, Z, H), governed by the magnitude of $V_{\mu N}$. The

relevant interaction terms are:

$$\mathcal{L}_{\mu WN} = \frac{g}{\sqrt{2}} W_\mu^- \bar{\mu} \gamma^\mu P_L V_{\mu N} N + \text{H.c.}, \quad (3)$$

$$\mathcal{L}_{\nu_\mu ZN} = \frac{g}{2 \cos \theta_w} Z_\mu \bar{\nu}_\mu \gamma^\mu P_L V_{\mu N} N + \text{H.c.}, \quad (4)$$

$$\mathcal{L}_{\nu_\mu HN} = \frac{M_N}{v} H \bar{\nu}_\mu P_R V_{\mu N} N + \text{H.c.} \quad (5)$$

III. DECAY MODES

In this section, we briefly explain the plausible decay modes of sLQ and RHN depending on the couplings mentioned above. A detailed explanation of these decay modes and their expressions is given in [30].

1. **Leptoquark Decays:** The branching ratios of $\tilde{R}_2^{2/3}$ into the uN and $d\mu$ final states as functions of the Yukawa coupling Y_{12} have been studied in detail in [30] for the benchmark choice $M_N = 50$ GeV. In the regime $M_{\tilde{R}_2^{2/3}} > M_N$ and a large Z_{11} , the two-body decay $\tilde{R}_2^{2/3} \rightarrow uN$ competes with the SM-like mode $\tilde{R}_2^{2/3} \rightarrow \mu d$. Owing to the large mass hierarchy between the sLQ and the SM fermions, the branching ratios are primarily governed by the relative sizes of the Yukawa couplings: the charged-lepton channel increases with Y_{12} and decreases with Z_{11} , while the RHN channel exhibits the complementary behavior.
2. **Right-Handed Neutrino Decays:** The RHN can decay via two qualitatively different mechanisms: through its mixing with SM neutrinos, giving rise to three-body decays mediated by off-shell W , Z , and Higgs bosons for lighter N , and through off-shell LQ exchange. For heavier N , the former decay mode will get replaced by on-shell two-body decays, such as $N \rightarrow lW, \nu Z, \nu H$. The relative importance of these channels depends crucially on the active-sterile mixing $V_{\mu N}$, the respective Yukawa couplings, and the sLQ mass. A detailed discussion of the corresponding branching-ratio patterns for representative benchmark choices (including $M_N = 50$ GeV) can be found in [30]. In general, for large mixing the electroweak-mediated channels dominate and the branching ratios are largely insensitive to the LQ mass, whereas for very small mixing the LQ-mediated modes become dominant, yielding sizable hadronic final states. For intermediate mixing values, both contributions are relevant, leading to a smooth transition in the decay pattern with increasing LQ mass.

IV. LQ PRODUCTION AT THE HL-LHC

In this section, we describe the various \tilde{R}_2 production channels at the HL-LHC that yield same sign dimuon

and multi-jet signatures. To realize this final state, we consider scenarios where at least one sLQ decays into a jet and a RHN. Crucially, the Majorana nature of the RHN allows it to decay into either μ^+ plus jets or μ^- plus jets with equal probability; this inherent lepton number violation provides a natural mechanism for generating same sign dilepton events. Furthermore, the Majorana character of the RHN, coupled with the charge-asymmetric initial state of a collider, facilitates additional production modes for that were not present in our previous study [30]. Representative parton-level Feynman diagrams for both single and pair production are illustrated in Fig. 1. Below, we provide an exhaustive list of all relevant pair and single production channels, together with their coupling dependence,

1. Pair Production:

- Similar to our previous work [30], we consider the pair production process $pp \rightarrow \tilde{R}_2 \tilde{R}_2$ (where, $\tilde{R}_2 \in \{\tilde{R}_2^{2/3}, \tilde{R}_2^{-1/3}\}$), mediated by a s -channel γ/Z boson or gluon. The representative Feynman diagrams for these channels are shown in Figs. 1a and 1c. In a hadron collider, we also have the mixed pair production channel $pp \rightarrow \tilde{R}_2^{\pm 2/3} \tilde{R}_2^{\pm 1/3}$ mediated by a s -channel W boson, as illustrated in Fig. 1b.
- In addition to the SM mediated pair production channels, pair production of \tilde{R}_2 mediated by the new physics couplings (Y_{12} and Z_{11}) is also possible. The process $pp \rightarrow \tilde{R}_2^{2/3} \tilde{R}_2^{-2/3}$ ($\tilde{R}_2^{1/3} \tilde{R}_2^{-1/3}$) can occur via t -channel $[\mu, N]$ ($[v, N]$) (See Fig. 1d). The cross section contribution involving t -channel SM fermions scale as Y_{12}^4 , whereas the contribution involving t -channel N scales as Z_{11}^4 .
- There is also interference between the relevant SM-mediated and new-

physics-mediated diagrams. For example, interference arises between the SM mediated pair production of $\tilde{R}_2^{2/3} \tilde{R}_2^{-2/3}$ and $\tilde{R}_2^{-1/3} \tilde{R}_2^{1/3}$ and the corresponding processes mediated by a t -channel v, μ, N . The cross section contribution from these interference terms scales as Y_{12}^2/Z_{11}^2 .

- If the pair production of \tilde{R}_2 proceeds only via a t -channel Majorana type N , a rich set of additional pair production channels becomes accessible, all of which can lead to the same sign dimuon plus multijet final state (See Fig. 1e). These channels do not interfere with the SM-mediated processes, and their cross sections scale as Z_{11}^4 . The relevant channels are $\tilde{R}_2^{\pm 2/3} \tilde{R}_2^{\pm 2/3}$, $\tilde{R}_2^{\pm 1/3} \tilde{R}_2^{\pm 1/3}$, $\tilde{R}_2^{\pm 2/3} \tilde{R}_2^{\mp 1/3}$, and $\tilde{R}_2^{\pm 2/3} \tilde{R}_2^{\pm 1/3}$.
- Following pair production, sLQs are decayed according to two distinct topologies to reach the targeted final states: Symmetric mode, where both decay into a RHN and a jet, and an asymmetric mode, where one yields an RHN and a jet while the other produces a muon and a jet. These production channels are detailed in Eqs. 6 and 8, respectively.

2. **Single Production:** In the single production mode, a \tilde{R}_2 is produced alongside a quark and a SM lepton or RHN. To obtain a same sign dimuon and multijet final state in single production, at least one of the produced sLQs must decay into an RHN. We present the symmetric and asymmetric single production modes in Eqs. 7 and 9, respectively. The representative Feynman diagrams for these processes are shown in Figs. 1f, 1g, 1h, and 1i.

Symmetric mode: Pair production

$$pp \rightarrow \left\{ \begin{array}{l} \tilde{R}_2^{+2/3} \tilde{R}_2^{-2/3}, \tilde{R}_2^{-2/3} \tilde{R}_2^{-2/3} \\ \tilde{R}_2^{+2/3} \tilde{R}_2^{+2/3}, \tilde{R}_2^{+1/3} \tilde{R}_2^{-1/3} \\ \tilde{R}_2^{+1/3} \tilde{R}_2^{+1/3}, \tilde{R}_2^{-1/3} \tilde{R}_2^{-1/3} \\ \tilde{R}_2^{+2/3} \tilde{R}_2^{-1/3}, \tilde{R}_2^{+2/3} \tilde{R}_2^{+1/3} \\ \tilde{R}_2^{-2/3} \tilde{R}_2^{-1/3}, \tilde{R}_2^{-2/3} \tilde{R}_2^{+1/3} \end{array} \right\} \rightarrow (jN)(jN) \rightarrow j(\mu jj) j(\mu jj) \equiv \mu^\pm \mu^\pm + N_{jet} \geq 6 \quad (6)$$

Here, j could either be a light quark or an anti quark or a gluon depending on the charge of $\tilde{R}_2^{2/3}$ or $\tilde{R}_2^{-1/3}$.

Symmetric mode: Single Production

$$pp \rightarrow \left\{ \begin{array}{l} \tilde{R}_2^{+2/3} jN, \tilde{R}_2^{-2/3} jN \rightarrow (jN) jN, (jN) jN \rightarrow j(\mu jj) j(\mu jj) \equiv \mu^\pm \mu^\pm + N_{jet} \geq 6 \\ \tilde{R}_2^{+1/3} jN, \tilde{R}_2^{-1/3} jN \rightarrow (jN) jN, (jN) jN \rightarrow j(\mu jj) j(\mu jj) \equiv \mu^\pm \mu^\pm + N_{jet} \geq 6 \end{array} \right\} \quad (7)$$

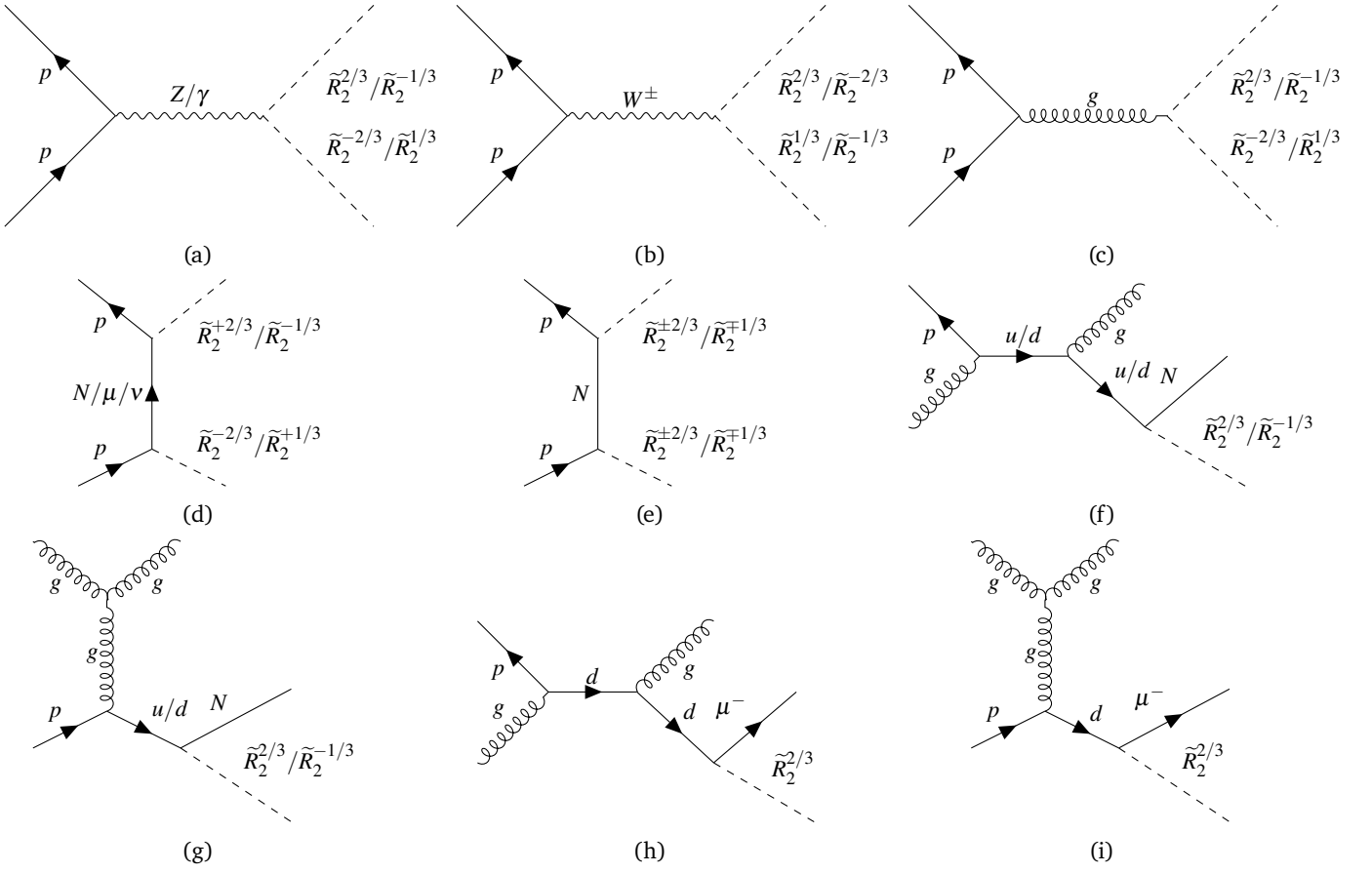


FIG. 1: Representative Feynman diagrams illustrating the pair and single production of \tilde{R}_2 .

Asymmetric mode: Pair production

$$pp \rightarrow \left\{ \begin{array}{l} \tilde{R}_2^{+2/3} \tilde{R}_2^{-2/3}, \tilde{R}_2^{-2/3} \tilde{R}_2^{-2/3} \\ \tilde{R}_2^{+2/3} \tilde{R}_2^{+2/3}, \tilde{R}_2^{+2/3} \tilde{R}_2^{-1/3} \\ \tilde{R}_2^{+2/3} \tilde{R}_2^{+1/3}, \tilde{R}_2^{-2/3} \tilde{R}_2^{-1/3} \\ \tilde{R}_2^{-2/3} \tilde{R}_2^{+1/3} \end{array} \right\} \rightarrow (jN)(j\mu) \rightarrow j(\mu jj) j\mu \equiv \mu^\pm \mu^\pm + N_{jet} \geq 4 \quad (8)$$

Asymmetric mode: Single production

$$pp \rightarrow \left\{ \begin{array}{l} \tilde{R}_2^{+2/3} \mu j, \tilde{R}_2^{-2/3} \mu j \rightarrow (jN) \mu j, (jN) \mu j \rightarrow j(\mu jj) j\mu \equiv \mu^\pm \mu^\pm + N_{jet} \geq 4 \\ \tilde{R}_2^{+2/3} jN, \tilde{R}_2^{-2/3} jN \rightarrow (j\mu) jN, (j\mu) jN \rightarrow j\mu j(\mu jj) \equiv \mu^\pm \mu^\pm + N_{jet} \geq 4 \end{array} \right\}. \quad (9)$$

In Fig. 2, we present the production cross sections as functions of $M_{\tilde{R}_2}$ for the channels discussed above at the HL-LHC, assuming the benchmark choice $Y_{12} = Z_{11} = 1$. Throughout the figure, we show only the parton-level production cross sections of \tilde{R}_2 . The salient features of

the plot are discussed below:

- The pair production channels $\tilde{R}_2^{2/3} \tilde{R}_2^{-2/3}$ and $\tilde{R}_2^{-1/3} \tilde{R}_2^{1/3}$ are shown by the solid red and blue curves, respectively. Unlike [30], where the SM

mediated, new-physics mediated, and interference contributions were displayed separately, here we present the total cross section for each channel as a single contour. We observe that the cross section for the $\tilde{R}_2^{2/3}\tilde{R}_2^{-2/3}$ channel is slightly larger than that for $\tilde{R}_2^{-1/3}\tilde{R}_2^{1/3}$. The SM and new-physics contributions involving a t -channel μ (ν) mediator for $\tilde{R}_2^{2/3}$ ($\tilde{R}_2^{-1/3}$) pair production, as well as the corresponding interference terms, are identical for these two modes. The observed difference arises from the pair production diagrams mediated by a t -channel N . In this case, the initial-state quark is an up quark for $\tilde{R}_2^{2/3}$ production and a down quark for $\tilde{R}_2^{-1/3}$ production. Since the parton distribution function (PDF) of the up quark inside the proton is significantly larger than that of the down quark, the contribution from this diagram enhances the cross section for $\tilde{R}_2^{2/3}\tilde{R}_2^{-2/3}$ production.

- The pair production cross sections for $\tilde{R}_2^{2/3}\tilde{R}_2^{2/3}$ and $\tilde{R}_2^{-1/3}\tilde{R}_2^{-1/3}$ are larger than those for $\tilde{R}_2^{-2/3}\tilde{R}_2^{-2/3}$ and $\tilde{R}_2^{1/3}\tilde{R}_2^{1/3}$, respectively. This behavior can be understood from the structure of the initial-state partons. The initial-state quark for $\tilde{R}_2^{2/3}\tilde{R}_2^{2/3}$ ($\tilde{R}_2^{-1/3}\tilde{R}_2^{-1/3}$) pair production is the up (down) quark, whereas for $\tilde{R}_2^{-2/3}\tilde{R}_2^{-2/3}$ ($\tilde{R}_2^{1/3}\tilde{R}_2^{1/3}$) production the initial state involves the anti-up (anti-down) quark. Since the PDF of an up (anti-up) quark is larger than that of a down (anti-down) quark in the proton, the corresponding cross sections exhibit the observed hierarchy. A similar argument applies to mixed-charge channels such as $\tilde{R}_2^{1/3}\tilde{R}_2^{2/3}$ and $\tilde{R}_2^{-1/3}\tilde{R}_2^{-2/3}$.
- In this section, we identify three primary single production channels contributing to the targeted signal topology: $\tilde{R}_2^{2/3}Nj$, $\tilde{R}_2^{-1/3}Nj$, and $\tilde{R}_2^{2/3}\mu j$. The corresponding Feynman diagrams, focusing on the dominant quark- and gluon-initiated subprocesses, are illustrated in Figs. 1f, 1g, 1h, and 1i. Among these, the $\tilde{R}_2^{2/3}Nj$ channel exhibits the largest cross section, exceeding that of $\tilde{R}_2^{-1/3}Nj$ by approximately a factor of two. This disparity is driven by the proton's PDFs; specifically, the $\tilde{R}_2^{2/3}Nj$ mode is initiated by up-quarks, whereas the $\tilde{R}_2^{-1/3}Nj$ mode originates from down-quarks. The former is thus enhanced by the valence u -quark density at the LHC. We further note that the cross section for the $\tilde{R}_2^{2/3}\mu j$ channel follows a numerical trend comparable to that of $\tilde{R}_2^{-1/3}Nj$.

V. SEARCH STRATEGY FOR \tilde{R}_2 AT THE HL-LHC

In Fig. 3, we present the kinematic distributions of the transverse momentum of the leading jet (p_T^j) and (H_T)

for both signal and background processes. Here, H_T is defined as the scalar sum of the transverse momenta of all visible particles,

$$H_T = \sum_{\text{jets}} p_T^{\text{jet}} + \sum_{\text{muons}} p_T^{\mu}. \quad (10)$$

The choice of these kinematic observables is motivated by the clear separation they provide between signal and background event distributions. We present the distributions separately for the symmetric and asymmetric modes of LQ production, including both pair and single production, for the benchmark scenario with $M_{\tilde{R}_2^{2/3}} = 1$ TeV and $M_N = 50$ GeV. The kinematic distributions for $\tilde{R}_2^{\mp 1/3}$ are largely similar to those of $\tilde{R}_2^{\pm 2/3}$, except in the case of asymmetric production where they do not contribute. For this reason, we do not present them separately.

- The green and blue curves in Fig. 3a correspond to the symmetric and asymmetric pair production modes, respectively. In both production modes, the leading jet originates from the decay of a $\tilde{R}_2^{2/3}$. Consequently, its transverse momentum distribution exhibits a peak around $M_{\tilde{R}_2^{2/3}}/2$, which for $M_{\tilde{R}_2^{2/3}} = 1$ TeV corresponds to approximately 500 GeV. This feature is common to both the symmetric and asymmetric production modes.
- The brown and red curves in Fig. 3a represent the symmetric and asymmetric single production modes, respectively. In single production, only one heavy particle with mass $M_{\tilde{R}_2} = 1$ TeV is produced, while the remaining energy in the event is shared with a relatively light recoil system. This redistribution of energy among lighter final-state particles leads to a softer p_T spectrum for the leading jet compared to pair production, where the leading jet predominantly arises from the decay of a second, equally heavy \tilde{R}_2 .
- In figure 3b, we present the H_T distributions for the pair production processes, where the symmetric and asymmetric production modes are shown by the green and blue curves, respectively. In the symmetric production mode, both LQs are produced with similar transverse momentum. Since the produced RHN decays entirely into visible final states, nearly the full energy of each LQ is transferred to jets and a muon. As can be seen from the figure, this results in a peak in H_T distribution around $2M_{\tilde{R}_2} \simeq 2$ TeV, with the maximum occurring around 2.3 TeV. In contrast, for the asymmetric production mode, the H_T distribution peaks at a slightly lower value, around 2.1 TeV. This reduction can be understood from the fact that only one of the produced LQs undergoes the decay chain involving the RHN. As a result, the visible final-state

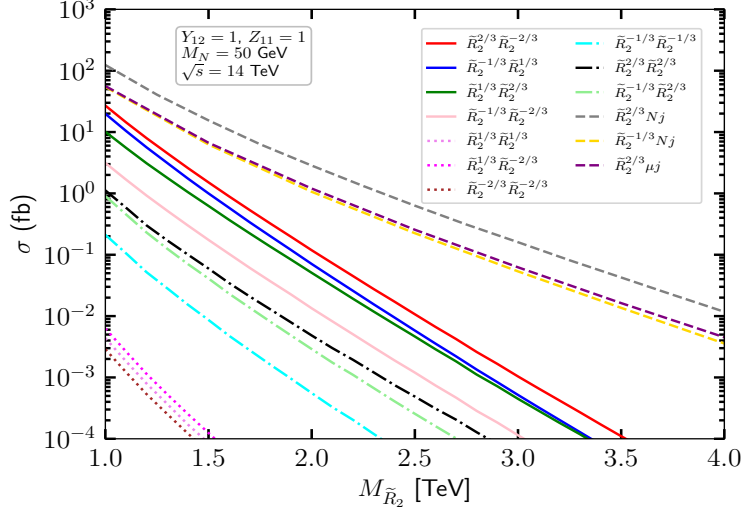


FIG. 2: Variation of the production cross section for different \tilde{R}_2 pair and single production channels as a function of $M_{\tilde{R}_2}$ at HL-LHC with C.O.M energy $\sqrt{s} = 14$ TeV. The Yukawa couplings are fixed to $Z_{11} = Y_{12} = 1$. The legend in the figure identifies the individual production modes.

multiplicity is reduced, leading to a comparatively smaller overall scalar sum.

- The brown and red curves in figure 3b represent the H_T distributions for the symmetric and asymmetric single production modes, respectively. In the symmetric single production case, the H_T distribution peaks at a significantly lower value, around 1.6 TeV. This behaviour is expected, since only one heavy LQ is produced, and therefore the visible transverse momentum is primarily governed by a single ~ 1 TeV resonance together with its recoil momentum. The associated RHN and the accompanying recoil jet typically carry comparatively softer transverse momenta, resulting in a substantially smaller overall scalar sum than in the pair production scenarios. In the asymmetric single production mode, the reduction in the number of visible final-state particles further suppresses the total transverse activity. Consequently, the H_T distribution peaks at an even lower value, around 1.2 TeV.

After analyzing the kinematic distributions shown in Fig. , we implement the following set of cuts, which provide effective discrimination between signal and background processes.

- The number of muons and jets: $N_{\text{muon}} = 2$ with same charge and $N_{\text{jet}} \geq 4$. We do not demand any specific isolation criterion for the muon. We apply base level cut on the muon transverse momentum, $p_T^\mu = 20$ GeV.
- b veto: number of b -jets $N_b = 0$ to suppress $t\bar{t}$ backgrounds.
- Among the jets, $N_{\text{jets}}(p_T^j > 200 \text{ GeV}, \Delta R_{\mu j} > 0.4) \geq 2$.

- $H_T > 2000$ GeV.

Background processes

In this section, we enumerate the SM background processes that can mimic the signal topology of same sign dimuons accompanied by multiple jets. For a detailed description of the background nomenclature, we refer the reader to Ref. [30]. The relevant background categories are summarized below.

1. VVV : Triboson production constitutes one of the dominant SM backgrounds for our signal topology. The relevant triboson combinations include $Z_\ell Z_\ell Z_h$, $W_\ell W_h Z_\ell$, $W_\ell W_\ell W_\ell$, and $W_\ell Z_\ell Z_h$. Here, the subscripts ℓ and h denote leptonic decays ($W \rightarrow \mu\nu$ or $Z \rightarrow \mu^+\mu^-$) and hadronic decays ($V \rightarrow jj$) of the gauge bosons, respectively. These processes typically yield more than two muons in the final state and can therefore contribute to same sign dimuon signatures. The accompanying multiple jets arise either from hadronic gauge-boson decays or from additional QCD radiation during parton showering and hadronization.
2. $VV + \text{jets}$: In the diboson plus jets category, the dominant background contributions arise from the processes $W_\ell Z_\ell + \text{jets}$ and $Z_\ell Z_\ell + \text{jets}$. The leptonic decays of the gauge bosons produce multiple muons in the final state, while the required jet multiplicity is supplied by hard QCD radiation as well as parton showering effects.
3. $t\bar{t}V$: This background category includes two distinct classes of processes. The first consists of $t_\ell \bar{t}_h W_\ell^+$ and $t_h \bar{t}_\ell W_\ell^-$. In these channels, the leptonic decay of the top (antitop) quark produces a b (\bar{b})

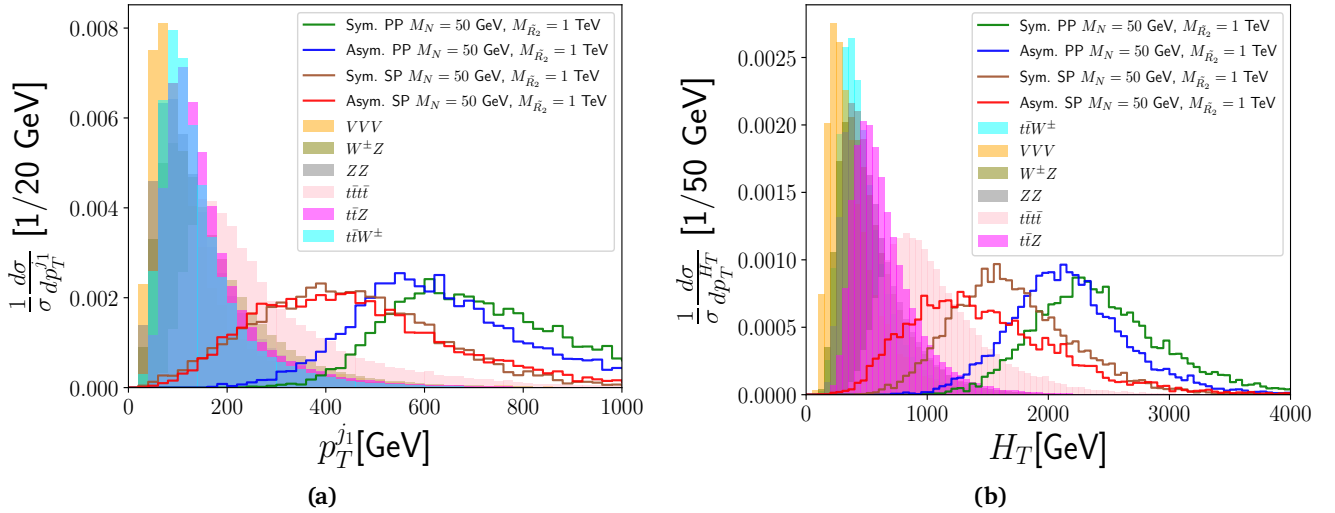


FIG. 3: Distributions of (a) the transverse momentum of the leading jet (p_T^{j1}) and (b) H_T for benchmark values of $M_{R_2} = 1$ TeV and $M_N = 50$ GeV in HL-LHC.

quark and a W^+ (W^-) boson, with the W subsequently decaying leptonically to $\mu^+ \nu$ ($\mu^- \bar{\nu}$). The additional W^+ (W^-) boson produced in association with the $t\bar{t}$ pair ensures the presence of same sign dimuons in the final state, while the hadronic decay of the remaining top quark provides additional jets. The second class corresponds to the process $t_h \bar{t}_\ell Z_\ell$. In this case, the leptonic decays of the top quark and the Z boson yield at least three muons in the final state, which can mimic the signal topology upon appropriate event selection. The required jet activity arises from the hadronic decay of the remaining top quark and additional QCD radiation.

4. $t\bar{t}t\bar{t}$: We consider all possible decay configurations of the four top quarks that can contribute to the signal-like final state. Purely hadronic decay modes, such as $t_h \bar{t}_h t_h \bar{t}_h$, do not produce leptons and therefore do not constitute a relevant background. In contrast, decay modes such as $t_h \bar{t}_\ell t_\ell \bar{t}_h$ lead to multiple muons in the final state and can mimic the same sign dimuon signature. Similarly, configurations like $t_\ell \bar{t}_h t_\ell \bar{t}_h$ can also produce same sign dimuons, with the accompanying jets arising from the hadronic decays of the remaining top quarks.

In addition to the dominant backgrounds discussed above, diboson (VV) and ditop ($t\bar{t}$) processes can, in principle, contribute to the same-sign dilepton signal topology through charge misidentification. For instance, diboson channels such as $W_h Z_\ell$ and $Z_h Z_\ell$ may yield opposite-sign dileptons at parton level; however, if the charge of one lepton is misidentified, these events can mimic a same-sign dilepton final state. A similar situation arises in ditop production, where configurations such as $t_\ell \bar{t}_\ell$ produce opposite-sign leptons, but charge misreconstruction of one lepton could lead to an apparent same-sign signature. In our analysis, we have not in-

cluded such effects. After applying realistic charge identification criteria and incorporating the corresponding misidentification probabilities, we find that the resulting contribution from these channels is negligible. Furthermore, the implementation of a b -jet veto substantially suppresses the ditop background, rendering its residual impact on the signal region insignificant.

VI. ANALYSIS FOR HL-LHC

In this section, we describe the methodology used to calculate the significance of the signal topology. For each case, the statistical significance \mathcal{Z} is calculated using the following expression outlined in [32],

$$\mathcal{Z} = \sqrt{2(N_S + N_B) \ln \left(\frac{N_S + N_B}{N_B} \right)} - 2N_S, \quad (11)$$

Here, N_S and N_B are the number of signal and background events, respectively. The background events are computed as follows,

$$N_B = \left(\sum_i \sigma_B^i \times \epsilon_B^i \right) \times \mathcal{L}, \quad (12)$$

Here, σ_B^i and ϵ_B^i denote the cross section and cut efficiency of the i^{th} background process, respectively. \mathcal{L} is the luminosity of the HL-LHC. The number of signal events N_S is parameterized in the following manner. N_S comprises of events from pair (symmetric and asymmetric) and single production (symmetric and asymmetric) modes. The number of signal events is given as,

$$N_S = N_{\text{sym}}^{\text{pair}} + N_{\text{sym}}^{\text{single}} + N_{\text{asym}}^{\text{pair}} + N_{\text{asym}}^{\text{single}}, \quad (13)$$

Here, $N_{\text{sym}}^{\text{pair}}$ ($N_{\text{asym}}^{\text{pair}}$) and $N_{\text{sym}}^{\text{single}}$ ($N_{\text{asym}}^{\text{single}}$) correspond to signal events from the symmetric (asymmetric) pair and

single production modes, respectively. We write $N_{\text{sym}}^{\text{pair}}$, $N_{\text{asym}}^{\text{pair}}$, $N_{\text{sym}}^{\text{single}}$, and $N_{\text{asym}}^{\text{single}}$ as follows,

$$N_{\text{sym}}^{\text{pair}} = \sigma_{\text{sym}}^{\text{pair}} \times \epsilon_{\text{sym}}^{\text{pair}} \times \beta^2(\tilde{R}_2 \rightarrow Nj) \times \beta^2(N \rightarrow \mu jj) \times \mathcal{L} \quad (14)$$

$$N_{\text{asym}}^{\text{pair}} = 2 \times \sigma_{\text{asym}}^{\text{pair}} \times \epsilon_{\text{asym}}^{\text{pair}} \times \beta(\tilde{R}_2 \rightarrow \mu j) \times \beta(\tilde{R}_2 \rightarrow Nj) \times \beta(N \rightarrow \mu jj) \times \mathcal{L} \quad (15)$$

$$N_{\text{sym}}^{\text{single}} = \sigma_{\text{sym}}^{\text{single}}(pp \rightarrow \tilde{R}_2 Nj) \times \epsilon_{\text{sym}}^{\text{single}} \times \beta(\tilde{R}_2 \rightarrow Nj) \times \beta^2(N \rightarrow \mu jj) \times \mathcal{L} \quad (16)$$

$$N_{\text{asym}}^{\text{single}} = \sigma_{\text{asym}}^{\text{single}}(pp \rightarrow \tilde{R}_2 Nj / \tilde{R}_2 \mu j) \times \epsilon_{\text{asym}}^{\text{single}} \times \beta(\tilde{R}_2 \rightarrow Nj / \mu j) \times \beta(N \rightarrow \mu jj) \times \mathcal{L} \quad (17)$$

Here, β corresponds to the BR. $\epsilon_{\text{sym}}^{\text{pair}}$ ($\epsilon_{\text{asym}}^{\text{pair}}$) and $\epsilon_{\text{sym}}^{\text{single}}$ ($\epsilon_{\text{asym}}^{\text{single}}$) are the efficiencies of the symmetric (asymmetric) pair and single production modes, respectively.

In Eqs. 6 and 8, we have listed all the possible production channels of \tilde{R}_2 , whose decay modes can lead to the desired final state. The cross section parameterization of the symmetric pair production modes is as follows,

$$\begin{aligned} \sigma_{\text{sym}}^{\text{pair}} = & \sigma(\tilde{R}_2^{2/3} \tilde{R}_2^{-2/3}) + \sigma(\tilde{R}_2^{-2/3} \tilde{R}_2^{-2/3}) + \sigma(\tilde{R}_2^{2/3} \tilde{R}_2^{2/3}) \\ & + \sigma(\tilde{R}_2^{1/3} \tilde{R}_2^{-1/3}) + \sigma(\tilde{R}_2^{1/3} \tilde{R}_2^{1/3}) + \sigma(\tilde{R}_2^{-1/3} \tilde{R}_2^{-1/3}) \\ & + \sigma(\tilde{R}_2^{2/3} \tilde{R}_2^{-1/3}) + \sigma(\tilde{R}_2^{2/3} \tilde{R}_2^{1/3}) + \sigma(\tilde{R}_2^{-2/3} \tilde{R}_2^{-1/3}) \\ & + \sigma(\tilde{R}_2^{-2/3} \tilde{R}_2^{-1/3}) + \sigma(\tilde{R}_2^{-2/3} \tilde{R}_2^{1/3}) \end{aligned} \quad (18)$$

and the parameterization of the asymmetric pair production modes is as follows,

$$\begin{aligned} \sigma_{\text{asym}}^{\text{pair}} = & \sigma(\tilde{R}_2^{2/3} \tilde{R}_2^{-2/3}) + \sigma(\tilde{R}_2^{-2/3} \tilde{R}_2^{-2/3}) + \sigma(\tilde{R}_2^{2/3} \tilde{R}_2^{2/3}) \\ & + \sigma(\tilde{R}_2^{2/3} \tilde{R}_2^{-1/3}) + \sigma(\tilde{R}_2^{2/3} \tilde{R}_2^{1/3}) \\ & + \sigma(\tilde{R}_2^{-2/3} \tilde{R}_2^{1/3}) \end{aligned} \quad (19)$$

This is to note that in the asymmetric production mode, we do not consider $\tilde{R}_2^{-1/3} \tilde{R}_2^{\pm 1/3}$ modes, as they will lead to final states involving missing energy from the decay $\tilde{R}_2^{-1/3} \rightarrow d\nu$, and not same-sign di-muon. The individual cross section are parameterized as follows,

$$\begin{aligned} \sigma(\tilde{R}_2^{2/3} \tilde{R}_2^{-2/3}) = & \sigma_{\tilde{R}_2^{2/3}}^{\text{QED}} + \sigma_{\tilde{R}_2^{2/3}}^{\text{QCD}} + Y_{12}^2 \left(\sigma_{\mu, \tilde{R}_2^{2/3}}^{\text{Int, QCD}} + \sigma_{\mu, \tilde{R}_2^{2/3}}^{\text{Int, QED}} \right) \\ & + Y_{12}^4 \sigma_{\tilde{R}_2^{2/3}}^{\mu} + Z_{11}^2 \left(\sigma_{N, \tilde{R}_2^{2/3}}^{\text{Int, QCD}} + \sigma_{N, \tilde{R}_2^{2/3}}^{\text{Int, QED}} \right) \\ & + Z_{11}^4 \sigma_{\tilde{R}_2^{2/3}}^N + Z_{11}^2 Y_{12}^2 \sigma_{\mu N, \tilde{R}_2^{2/3}}^{\text{Int}} \end{aligned} \quad (20)$$

$$\begin{aligned} \sigma(\tilde{R}_2^{1/3} \tilde{R}_2^{-1/3}) = & \sigma_{\tilde{R}_2^{-1/3}}^{\text{QED}} + \sigma_{\tilde{R}_2^{-1/3}}^{\text{QCD}} + Y_{12}^2 \left(\sigma_{\nu, \tilde{R}_2^{-1/3}}^{\text{Int, QCD}} + \sigma_{\nu, \tilde{R}_2^{-1/3}}^{\text{Int, QED}} \right) \\ & + Y_{12}^4 \sigma_{\tilde{R}_2^{-1/3}}^{\nu} + Z_{11}^2 \left(\sigma_{N, \tilde{R}_2^{-1/3}}^{\text{Int, QCD}} + \sigma_{N, \tilde{R}_2^{-1/3}}^{\text{Int, QED}} \right) \\ & + Z_{11}^4 \sigma_{\tilde{R}_2^{-1/3}}^N + Z_{11}^2 Y_{12}^2 \sigma_{\nu N, \tilde{R}_2^{-1/3}}^{\text{Int}} \end{aligned} \quad (21)$$

$$\begin{aligned} \sigma(\tilde{R}_2^{\pm 2/3} \tilde{R}_2^{\mp 1/3}) = & \sigma_{\tilde{R}_2^{\pm 2/3} \tilde{R}_2^{\mp 1/3}}^{\text{QED}} + Z_{11}^2 \sigma_{N, \tilde{R}_2^{\pm 2/3} \tilde{R}_2^{\mp 1/3}}^{\text{Int, QED}} \\ & + Z_{11}^4 \sigma_{\tilde{R}_2^{\pm 2/3} \tilde{R}_2^{\mp 1/3}}^N \end{aligned} \quad (22)$$

$$\sigma(\tilde{R}_2^{\pm 2/3} \tilde{R}_2^{\pm 2/3}) = Z_{11}^4 \sigma_{\tilde{R}_2^{\pm 2/3} \tilde{R}_2^{\pm 2/3}}^N \quad (23)$$

$$\sigma(\tilde{R}_2^{\pm 1/3} \tilde{R}_2^{\pm 1/3}) = Z_{11}^4 \sigma_{\tilde{R}_2^{\pm 1/3} \tilde{R}_2^{\pm 1/3}}^N \quad (24)$$

$$\sigma(\tilde{R}_2^{\pm 1/3} \tilde{R}_2^{\pm 2/3}) = Z_{11}^4 \sigma_{\tilde{R}_2^{\pm 1/3} \tilde{R}_2^{\pm 2/3}}^N \quad (25)$$

In the above equations, the various notations used for the production cross sections σ are defined as follows:

- $\sigma_{\tilde{R}_2^{2/3}}^{\text{QED}}$ ($\sigma_{\tilde{R}_2^{-1/3}}^{\text{QED}}$) and $\sigma_{\tilde{R}_2^{2/3}}^{\text{QCD}}$ ($\sigma_{\tilde{R}_2^{-1/3}}^{\text{QCD}}$) denote the pair production of $\tilde{R}_2^{2/3}$ ($\tilde{R}_2^{-1/3}$) mediated by an s -channel Z/γ boson and a gluon, respectively.
- $\sigma_{\tilde{R}_2^{2/3}}^{\mu}$ and $\sigma_{\tilde{R}_2^{-1/3}}^N$ refer to the pair production of $\tilde{R}_2^{2/3}$ and $\tilde{R}_2^{-1/3}$ mediated via a t -channel exchange of a μ and a N , respectively.
- $\sigma_{\mu, \tilde{R}_2^{2/3}}^{\text{Int, QCD}}$ denotes the interference contribution between the t -channel μ -mediated pair production of $\tilde{R}_2^{2/3}$ and the s -channel SM QCD-mediated pair production process. Similarly, $\sigma_{\mu, \tilde{R}_2^{2/3}}^{\text{Int, QED}}$ represents the interference between the t -channel μ -mediated and the s -channel SM QED-mediated pair production amplitudes. An analogous interpretation applies to $\sigma_{N, \tilde{R}_2^{-1/3}}^{\text{Int, QCD}}$ and $\sigma_{N, \tilde{R}_2^{-1/3}}^{\text{Int, QED}}$, with the only difference being that the t -channel mediator in this case is the RHN N .
- In Eq. 22, $\sigma_{\tilde{R}_2^{\pm 2/3} \tilde{R}_2^{\mp 1/3}}^{\text{QED}}$ denotes the pair production of $\tilde{R}_2^{\pm 2/3} \tilde{R}_2^{\mp 1/3}$ mediated by an s -channel W boson. The term $\sigma_{\tilde{R}_2^{\pm 2/3} \tilde{R}_2^{\mp 1/3}}^N$ corresponds to pair production via a t -channel exchange of N . The quantity $\sigma_{N, \tilde{R}_2^{\pm 2/3} \tilde{R}_2^{\mp 1/3}}^{\text{Int, QED}}$ represents the interference contribution between these two processes.
- The cross section contributions appearing in Eqs. 23, 24, and 25 arise exclusively from pair production processes mediated by a t -channel exchange of N .

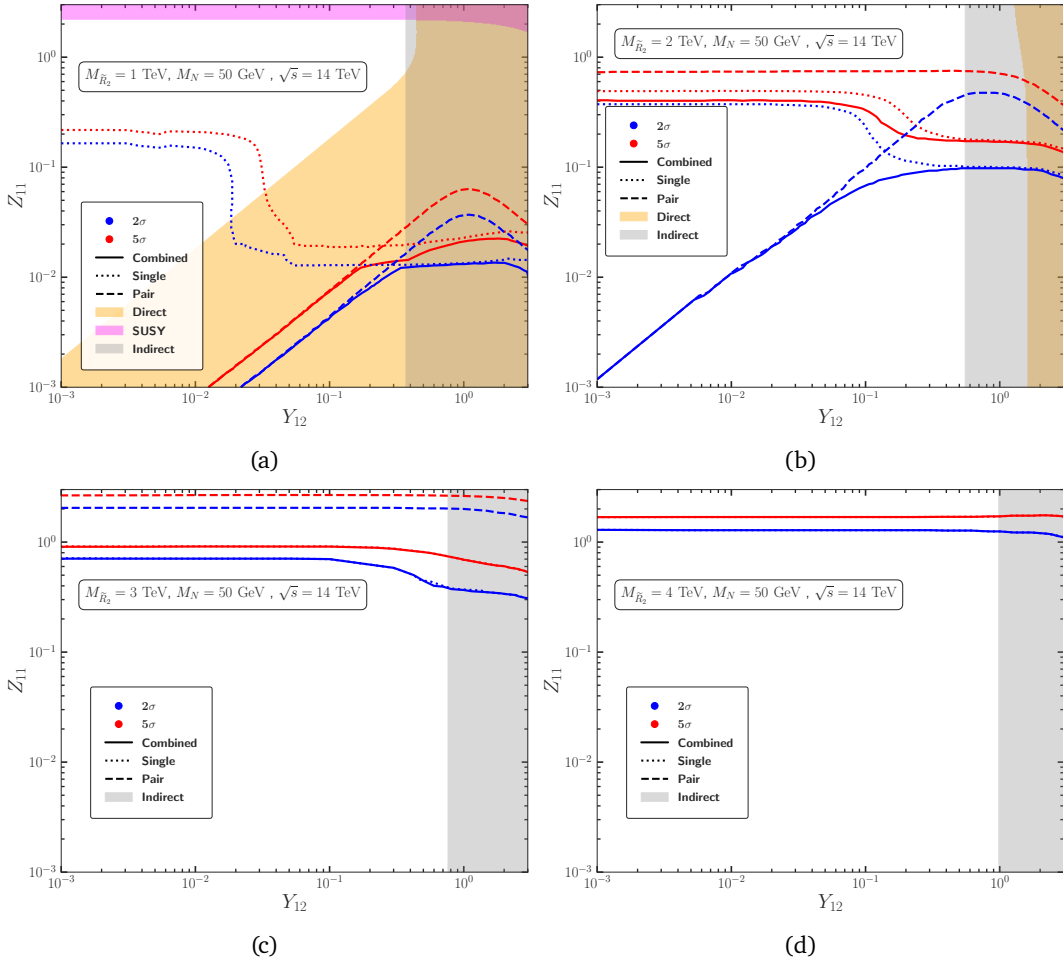


FIG. 4: Here, we show the contour plots for 2σ and 5σ statistical significance in the $Y_{12} - Z_{11}$ plane. We fix $M_N = 50$ GeV. (a); The mass of sLQ has been set to $\tilde{R}_2 = 1.0$ TeV. The yellow region is excluded by ATLAS direct search [12]. The pink region is excluded by ATLAS SUSY gluino direct search [33]. The gray region is excluded by the CMS indirect search [34]. (b) Here we consider, mass of $\tilde{R}_2 = 2.0$ TeV. (c) Here we consider, mass of $\tilde{R}_2 = 3.0$ TeV. (d) Here we consider, mass of $\tilde{R}_2 = 4.0$ TeV.

VII. RESULTS AND DISCUSSIONS

In Fig. 4, we present the projected sensitivity contours in the $Y_{12} - Z_{11}$ plane for few illustrative sLQ masses $M_{\tilde{R}_2} = 1.0, 2.0, 3.0,$ and 4.0 TeV, assuming $M_N = 50$ GeV and $\sqrt{s} = 14$ TeV. The dashed, dotted, and solid contours correspond to sensitivities obtained by considering pair production only, single production only, and their combined contribution, respectively. The blue (red) contours denote the 2σ sensitivity reach (5σ discovery reach). Existing constraints from the ATLAS direct LQ search [12], the ATLAS gluino-pair SUSY search [33], and indirect CMS LQ limits [34] are shown by the orange, pink, and gray shaded regions, respectively. The procedure used to recast these limits is described in detail in Ref. [30].

For $M_{\tilde{R}_2} = 1.0$ TeV, shown in Fig. 4a, the pair production contours corresponding to both the 2σ exclusion and 5σ discovery reach exhibit a linear and monotonically increasing dependence on the Yukawa

couplings Y_{12} and Z_{11} up to $Y_{12} \lesssim 1.0$. This behavior is governed by the structure of the signal yield, which factorizes into the total pair production cross section and the relevant BRs. For $M_{\tilde{R}_2} = 1.0$ TeV, the pair production cross section is dominated by QCD-mediated processes and is therefore largely insensitive to Y_{12} and Z_{11} . As a result, the BRs, $\text{BR}(\tilde{R}_2 \rightarrow \mu j)$ and $\text{BR}(\tilde{R}_2 \rightarrow N j)$ remain approximately constant, leading to the observed monotonic behavior of the sensitivity contours. For larger values of Y_{12} , the contours reach a maximum around $Y_{12} \simeq 1.0$ and subsequently turn over. This reversal arises from the increasing importance of Yukawa-induced contributions proportional to Y_{12}^4 in the pair production cross section (see Fig. 1d). In this regime, a smaller value of Z_{11} is sufficient to maintain a fixed statistical significance. Mild deviations from strict linearity also receive contributions from interference between SM s -channel amplitudes and Yukawa-mediated t -channel diagrams; however, these effects remain subdominant compared to the leading QCD contribution and do not qualitatively alter the overall trend.

VIII. CONCLUSIONS

The single production contours display a qualitatively different behavior. For $Z_{11} \simeq 0.2$ and $Y_{12} \lesssim 10^{-2}$, the contours are largely insensitive to variations in Y_{12} . This reflects the fact that single production is dominated by gluon–quark initiated processes that primarily depend on Z_{11} . As Y_{12} increases, the contours exhibit a pronounced dip, corresponding to an increase in $\text{BR}(\tilde{R}_2 \rightarrow \mu j)$ and a compensating reduction in the value of Z_{11} required to achieve a given significance. Once the BRs stabilize, the contours again become weakly dependent on Y_{12} . The combined production contours initially follow the pair production behavior but merge with the single production contours at larger values of the couplings, reflecting the transition between the two dominant production mechanisms.

In Fig. 4b, we show the corresponding results for $M_{\tilde{R}_2} = 2.0$ TeV. Compared to the 1.0 TeV case, the 2σ projection contours from pair and combined production retain a monotonic behavior, while the 5σ pair production contour becomes insensitive to Y_{12} for $Y_{12} < 1$ and requires $Z_{11} \sim \mathcal{O}(1)$. This reflects the reduced QCD pair production cross section at higher masses. Owing to the Majorana nature of the RHN, the contributions from the previously subdominant Z_{11} -dependent diagrams to pair production rises, allowing larger values of Z_{11} to partially compensate for phase-space suppression. For $Y_{12} \gtrsim 1$, Yukawa (Y_{12})-induced contributions become significant and lead to a downward turn in the contours. The single production contours retain the qualitative features observed at 1.0 TeV, albeit with a smoother dependence on Y_{12} . In this mass range, the 5σ combined contour closely follows the single production contour, indicating the reduced impact of pair production. The SUSY-inspired constraints no longer restrict the parameter space shown.

For $M_{\tilde{R}_2} = 3.0$ and 4.0 TeV, shown in Figs. 4c and 4d, respectively, the phenomenology changes qualitatively. In both cases, single production dominates the sensitivity, and the combined production contours overlap almost entirely with those from single production alone. Pair production contributes only for very large values of Z_{11} and remains insensitive to Y_{12} . In this regime, only indirect constraints are relevant. These results highlight the crucial role of single production and underscore the novelty and importance of the same sign dimuon channel in probing heavy sLQs.

We have presented a detailed phenomenological study of the sLQ \tilde{R}_2 in scenarios where it couples to lighter RHN state, motivated by well-established theoretical frameworks and by the limited sensitivity of existing searches to non-standard LQ decay modes. Focusing on the case in which the LQ is heavier than the RHN, we have identified the same sign dimuon plus multijet final state as a particularly clean and robust probe at the HL-LHC, benefiting from low SM backgrounds and direct sensitivity to lepton-number-violating signatures associated with a Majorana RHN.

Our analysis combines pair and single production mechanisms to assess the HL-LHC sensitivity over a wide range of LQ masses and Yukawa couplings. For LQ masses near 1–2 TeV and small Yukawa couplings, pair production—dominated by QCD interactions—provides the leading contribution to the projected sensitivity. As the LQ mass increases beyond 2.0 TeV, single production becomes increasingly important and eventually dominates the sensitivity, allowing the HL-LHC to probe regions of parameter space that would otherwise remain inaccessible. The combined analysis demonstrates a strong complementarity between the two production modes, significantly extending the reach in the Y_{12} – Z_{11} plane.

When compared with existing experimental constraints, we find that the same sign dimuon channel probes sizable regions of parameter space that are not excluded by current direct LQ searches, SUSY-inspired analyses, or indirect limits from high-mass dilepton measurements. In particular, for multi-TeV LQ masses where pair production is strongly suppressed, the HL-LHC retains meaningful sensitivity through single production, underscoring its unique capability to explore such scenarios.

Overall, our results demonstrate that sLQ with sizable couplings to RHNs remain a compelling and experimentally testable possibility at the HL-LHC. The search strategy developed here provides a concrete pathway to simultaneously probing LQ dynamics and the Majorana nature of RHNs. Extensions of this work to other flavor structures, RHN mass hierarchies, or complementary final states could further enhance the discovery potential at the HL-LHC and future collider facilities.

ACKNOWLEDGMENTS

The authors acknowledge the use of SAMKHYA: High-Performance Computing Facility provided by the Institute of Physics (IOP), Bhubaneswar.

[1] W. Buchmüller, R. Ruckl, and D. Wyler, “Leptoquarks in Lepton - Quark Collisions,” *Phys. Lett. B* **191** (1987)

442–448. [Erratum: *Phys.Lett.B* 448, 320–320 (1999)].

- [2] J. Blumlein, E. Boos, and A. Pukhov, “Leptoquark pair production at ep colliders,” *Mod. Phys. Lett. A* **9** (1994) 3007–3022, arXiv:hep-ph/9404321.
- [3] J. Blumlein, E. Boos, and A. Kryukov, “Leptoquark pair production in hadronic interactions,” *Z. Phys. C* **76** (1997) 137–153, arXiv:hep-ph/9610408.
- [4] I. Doršner, S. Fajfer, A. Greljo, J. Kamenik, and N. Košnik, “Physics of leptoquarks in precision experiments and at particle colliders,” *Phys. Rept.* **641** (2016) 1–68, arXiv:1603.04993 [hep-ph].
- [5] J. C. Pati and A. Salam, “Lepton Number as the Fourth Color,” *Phys. Rev. D* **10** (1974) 275–289. [Erratum: *Phys.Rev.D* **11**, 703–703 (1975)].
- [6] H. Georgi and S. Glashow, “Unity of All Elementary Particle Forces,” *Phys. Rev. Lett.* **32** (1974) 438–441.
- [7] B. Schrempp and F. Schrempp, “LIGHT LEPTOQUARKS,” *Phys. Lett. B* **153** (1985) 101–107.
- [8] R. Barbier *et al.*, “R-parity violating supersymmetry,” *Phys. Rept.* **420** (2005) 1–202, arXiv:hep-ph/0406039.
- [9] M. Kohda, H. Sugiyama, and K. Tsumura, “Lepton number violation at the LHC with leptoquark and diquark,” *Phys. Lett. B* **718** (2013) 1436–1440, arXiv:1210.5622 [hep-ph].
- [10] **Heavy Flavor Averaging Group (HFLAV)** Collaboration, S. Banerjee *et al.*, “Averages of b-hadron, c-hadron, and τ -lepton properties as of 2023,” *Phys. Rev. D* **113** no. 1, (2026) 012008, arXiv:2411.18639 [hep-ex].
- [11] T. Aoyama *et al.*, “The anomalous magnetic moment of the muon in the Standard Model,” *Phys. Rept.* **887** (2020) 1–166, arXiv:2006.04822 [hep-ph].
- [12] **ATLAS** Collaboration, G. Aad *et al.*, “Search for pairs of scalar leptoquarks decaying into quarks and electrons or muons in $\sqrt{s} = 13$ TeV pp collisions with the ATLAS detector,” *JHEP* **10** (2020) 112, arXiv:2006.05872 [hep-ex].
- [13] A. Bessaa and S. Davidson, “Constraints on t -channel leptoquark exchange from LHC contact interaction searches,” *Eur. Phys. J. C* **75** no. 2, (2015) 97, arXiv:1409.2372 [hep-ph].
- [14] T. Mandal, S. Mitra, and S. Raz, “ $R_{D^{(*)}}$ motivated \mathcal{S}_1 leptoquark scenarios: Impact of interference on the exclusion limits from LHC data,” *Phys. Rev. D* **99** no. 5, (2019) 055028, arXiv:1811.03561 [hep-ph].
- [15] **ATLAS** Collaboration, G. Aad *et al.*, “Search for new non-resonant phenomena in high-mass dilepton final states with the ATLAS detector,” *JHEP* **11** (2020) 005, arXiv:2006.12946 [hep-ex]. [Erratum: *JHEP* **04**, 142 (2021)].
- [16] K. S. Babu, P. S. B. Dev, S. Jana, and A. Thapa, “Unified framework for B -anomalies, muon $g - 2$ and neutrino masses,” *JHEP* **03** (2021) 179, arXiv:2009.01771 [hep-ph].
- [17] A. Bhaskar, D. Das, T. Mandal, S. Mitra, and C. Neeraj, “Precise limits on the charge-2/3 U1 vector leptoquark,” *Phys. Rev. D* **104** no. 3, (2021) 035016, arXiv:2101.12069 [hep-ph].
- [18] A. Angelescu, D. Bečirević, D. A. Faroughy, F. Jaffredo, and O. Sumensari, “Single leptoquark solutions to the B-physics anomalies,” *Phys. Rev. D* **104** no. 5, (2021) 055017, arXiv:2103.12504 [hep-ph].
- [19] **CMS** Collaboration, A. Hayrapetyan *et al.*, “Search for a third-generation leptoquark coupled to a τ lepton and a b quark through single, pair, and nonresonant production in proton-proton collisions at $\sqrt{s} = 13$ TeV,” *JHEP* **05** (2024) 311, arXiv:2308.07826 [hep-ex].
- [20] S. Mandal, M. Mitra, and N. Sinha, “Probing leptoquarks and heavy neutrinos at the LHeC,” *Phys. Rev. D* **98** no. 9, (2018) 095004, arXiv:1807.06455 [hep-ph].
- [21] R. Padhan, S. Mandal, M. Mitra, and N. Sinha, “Signatures of \tilde{R}_2 class of Leptoquarks at the upcoming ep colliders,” *Phys. Rev. D* **101** no. 7, (2020) 075037, arXiv:1912.07236 [hep-ph].
- [22] G. Cottin, O. Fischer, S. Mandal, M. Mitra, and R. Padhan, “Displaced neutrino jets at the LHeC,” *JHEP* **06** (2022) 168, arXiv:2104.13578 [hep-ph].
- [23] A. Bhaskar, Y. Chaurasia, K. Deka, T. Mandal, S. Mitra, and A. Mukherjee, “Right-handed neutrino pair production via second-generation leptoquarks,” *Phys. Lett. B* **843** (2023) 138039, arXiv:2301.11889 [hep-ph].
- [24] G. Duraikandan, R. Khanna, T. Mandal, S. Mitra, and R. Sharma, “Right-handed neutrino production through first-generation leptoquarks,” *Phys. Rev. D* **111** no. 7, (2025) 075032, arXiv:2412.19751 [hep-ph].
- [25] P. Minkowski, “ $\mu \rightarrow e\gamma$ at a Rate of One Out of 10^9 Muon Decays?,” *Phys. Lett. B* **67** (1977) 421–428.
- [26] M. Gell-Mann, P. Ramond, and R. Slansky, “Complex Spinors and Unified Theories,” *Conf. Proc. C* **790927** (1979) 315–321, arXiv:1306.4669 [hep-th].
- [27] R. N. Mohapatra and G. Senjanovic, “Neutrino Mass and Spontaneous Parity Nonconservation,” *Phys. Rev. Lett.* **44** (1980) 912.
- [28] T. Yanagida, “Horizontal gauge symmetry and masses of neutrinos,” *Conf. Proc. C* **7902131** (1979) 95–99.
- [29] T. Yanagida, “Horizontal Symmetry and Masses of Neutrinos,” *Prog. Theor. Phys.* **64** (1980) 1103.
- [30] S. Saha, A. Bhaskar, P. S. B. Dev, and M. Mitra, “Exploring Scalar Leptoquarks at Muon Collider via Indirect Signatures and Right-Handed Neutrino-Assisted Decays,” arXiv:2509.04579 [hep-ph].
- [31] G. Apollinari, O. Brüning, T. Nakamoto, and L. Rossi, “High Luminosity Large Hadron Collider HL-LHC,” *CERN Yellow Rep.* no. 5, (2015) 1–19, arXiv:1705.08830 [physics.acc-ph].
- [32] G. Cowan, K. Cranmer, E. Gross, and O. Vitells, “Asymptotic formulae for likelihood-based tests of new physics,” *Eur. Phys. J. C* **71** (2011) 1554, arXiv:1007.1727 [physics.data-an]. [Erratum: *Eur.Phys.J.C* **73**, 2501 (2013)].
- [33] **ATLAS** Collaboration, G. Aad *et al.*, “Search for pair production of squarks or gluinos decaying via sleptons or weak bosons in final states with two same-sign or three leptons with the ATLAS detector,” *JHEP* **02** (2024) 107, arXiv:2307.01094 [hep-ex].
- [34] **CMS** Collaboration, “Search for t -channel scalar and vector leptoquark exchange in the high mass dimuon and dielectron spectrum in proton-proton collisions at $\sqrt{s} = 13$ TeV,”.